

**THE EFFECT OF THERMAL OXIDATION ON
MONOCRYSTALLINE SILICON SOLAR CELL EFFICIENCY**

by

NURSANIYAH BINTI A WAHAB

**Thesis submitted in fulfilment of the requirements
for the degree of
Master of Science**

July, 2013

ACKNOWLEDGEMENT

Assalamualaikum w.b.t and selamat sejahtera.

First for all, I would like to thank to Allah s.w.t for giving me strength and opportunity to complete my master research. Secondly, I would like to record my gratitude to Associated Professor Dr. Sohail Aziz Khan, my supervisor for helping me so much during all these time in completing this research. His valuable guidance, advice, critics and supports really encouraged me to do the best for this research. I appreciate his willingness to share the knowledge in this field and honoured to be one of his students.

This thesis is a gift to my beloved parents (Hasmah binti Daud and A. Wahab bin Hashim). Terima kasih mak dan abah atas kasih sayang, semangat dan dorongan yang tidak berbelah-bahagi sepanjang Uda menyiapkan master ini. Thank you very much. Not forgetting my fiancee for giving me strength, support, motivation and always standing behind me during all these while. The neither extended in appreciation also giving to my family, dearest friends and all NOR Lab staffs for their helps throughout this research. Thank you everyone.

Nursaniyah binti A. Wahab

M.Sc Physics

Universiti Sains Malaysia

TABLE OF CONTENTS

ACKNOWLEDGMENT	ii
TABLE OF CONTENTS	iii
LIST OF TABLES	viii
LIST OF FIGURES	ix
LIST OF ABBREVIATIONS	xii
LIST OF SYMBOLS	xiv
ABSTRAK	xviii
ABSTRACT	xix
CHAPTER 1 – INTRODUCTION	1
1.1 Renewable Energy Sources.....	1
1.2 The Role of Solar Photovoltaic Energy.....	3
1.3 Scope of Study.....	6
1.4 Research Objectives.....	6
1.5 Thesis Organization.....	7
CHAPTER 2 - LITERATURE REVIEW	8
2.0 Introduction.....	8
2.1 Genealogy of Silicon Solar Cell.....	8
2.2 Surface Passivation.....	11
2.3 Thin Passivating Oxide Film.....	11
2.4 Rear Passivating Back Surface Field.....	13
2.5 Summary.....	14

CHAPTER 3 – THEORY	15
3.0 Introduction.....	15
3.1 Theory of Silicon.....	15
3.2 Theory of Solar Cell.....	17
3.2.1 The <i>p-n</i> Junction.....	17
3.2.2 The <i>p-n</i> Junction at Equilibrium.....	18
3.2.3 The <i>p-n</i> Junction at Non-Equilibrium.....	20
3.2.4 The <i>p-n</i> Junction under Illumination.....	21
3.3 Photovoltaic Effect.....	22
3.4 Air Mass and Solar Spectrum.....	23
3.4.1 Air Mass.....	23
3.4.2 Solar Spectrum.....	24
3.5 Solar Cell Characteristics.....	25
3.5.1 Solar Cell Parameters.....	25
3.5.2 Illuminated Current-Voltage (<i>I-V</i>) Characteristics.....	27
3.6 Recombination Mechanisms.....	28
3.6.1 Radiative Recombination.....	29
3.6.2 Auger Recombination.....	30
3.6.3 Shockley-Read-Hall Recombination.....	32
3.6.3(a) Shockley-Read-Hall Recombination in Bulk.....	32
3.6.3(b) Shockley-Read-Hall Recombination at Surface.....	33
3.7 Reduction in Surface Recombination.....	34
3.7.1 Passivated Front Surface.....	34
3.7.2 Reduction of Electrons and Holes Surface Concentration.....	35
3.8 The Effective Lifetime.....	35

3.9	Theory of Surface Passivation.....	36
3.9.1	Silicon Dioxide Thermally Grown on Front Surface.....	36
3.9.2	Passivation at Rear Surface.....	37
3.10	Summary.....	38
CHAPTER 4 - METHODOLOGY AND EQUIPMENTS.....		39
4.0	Introduction.....	39
4.1	RCA Clean.....	39
4.2	Cutting Wafer.....	40
4.3	Measurement of Resistivity.....	41
4.4	Thinning Wafer.....	42
4.4.1	Piranha Clean.....	43
4.5	Diffusion System.....	43
4.5.1	Phosphorus Emitter (<i>N</i> -type) Diffusion.....	44
4.5.1(a)	Pre-deposition Step.....	44
4.5.1(b)	Drive-in Step.....	45
4.6	Thermal Oxidation.....	46
4.6.1	Dry Oxidation.....	46
4.6.2	Wet (Drive-in) Oxidation.....	47
4.7	Back Surface Field (BSF).....	48
4.8	Alloying.....	50
4.9	Lift-off Process.....	50
4.9.1	Photoresist for Lift-Off.....	51
4.9.2	Soft Baking.....	52
4.9.3	Photoresist Exposure.....	53
4.9.4	Photoresist Development Process.....	54

4.9.5	Hard Baking.....	54
4.9.6	Wet Chemical Etching.....	55
4.9.7	Metallization.....	55
4.9.8	Edge Shunt Isolation.....	58
4.9.9	Annealing.....	58
4.10	Measurements.....	59
4.10.1	Manual Measurement.....	59
4.10.2	Solar Simulator.....	60
4.10.3	SILVACO Simulation Software.....	60
4.11	Summary.....	61
CHAPTER 5 - RESULTS AND DISCUSSION.....		62
5.0	Introduction.....	62
5.1	Effects in Various Wet Etching Time to Si Wafer Thickness.....	62
5.1.1	Surface Morphology from Impact of Etching Process.....	66
5.1.2	Electric Properties.....	67
5.2	Effect in Various Times to Thin Passivating Oxide Layer Growth.....	69
5.3	Effect of Back Surface Field (BSF).....	72
5.3.1	Structural Properties after Alloying BSF.....	72
5.4	Effect of Lift-off Process to Contact Pattern.....	75
5.5	Edge Shunt Isolation.....	77
5.6	<i>I-V</i> Characterization of Si Solar Cell.....	80
5.6.1	Illuminated <i>I-V</i> Characteristics.....	80
5.7	Simulated Photocurrent Response.....	83
5.8	Summary.....	87

CHAPTER 6 - CONCLUSION AND FUTURE WORKS.....	88
6.1 Conclusion.....	88
6.2 Future Works.....	89
REFERENCES.....	90
APPENDICES.....	96
Appendix A.....	97
Appendix B.....	99
Appendix C.....	100
LIST OF PUBLICATION.....	103

LIST OF TABLES

Table 1.1	Renewable energy sources	2
Table 1.2	Overview and comparison of major PV technology	5
Table 4.1	Time required for deposition oxide layer on surface of Si wafers	47
Table 5.1	Mass of Si wafers before and after thinning process	63
Table 5.2	Thickness of Si wafers after thinning process	64
Table 5.3	Oxide thickness for thin passivation layer at temperature of 1000 °C	70
Table 5.4	Thickness of photoresist layer based on different at spin speed	75
Table 5.5	Photolithography processes	76
Table 5.6	V_{oc} and I_{sc} output after metal contact under incandescent lamp	77
Table 5.7	The sheet resistivity value for Si solar cell before and after edge shunt isolation process	78
Table 5.8	Summary of effect different in surface passivation layer thickness to Si solar cell efficiency	80
Table 5.9	SILVACO simulation value of short-circuit current and open-circuit voltage	86
Table 5.10	Short-circuit current and open-circuit voltage output from SILVACO software and solar simulator	86

LIST OF FIGURES

Figure 3.1	Tetrahedral crystal structure of crystalline silicon	16
Figure 3.2	The schematic diagram of energy bands for electrons in a semiconductor	16
Figure 3.3	The $p-n$ junction structure	18
Figure 3.4	Energy band diagram of a $p-n$ junction in thermal equilibrium	19
Figure 3.5	Schematic diagram of photovoltaic effect in solar cell	22
Figure 3.6	The air mass	23
Figure 3.7	Spectral irradiance of the sun under AM 0, AM 1.5G and AM 1.5D	24
Figure 3.8	$I-V$ curves for dark and illuminated conditions of solar cell	25
Figure 3.9	Equivalent circuit of solar cell	27
Figure 3.10	Carrier recombination mechanisms in semiconductors: a) radiative; b) SRH and c) Auger recombination	30
Figure 3.11	Plot of radiative, Auger, SRH and total lifetime versus injection level in 1.0 ohm.cm p -type semiconductor	35
Figure 3.12	The basic model for oxidation of silicon	37
Figure 4.1	The p -type $\langle 100 \rangle$ Si wafer	40
Figure 4.2	The diamond scriber	41
Figure 4.3	The four-point probe	41
Figure 4.4	Etch rates for 30% KOH solution [J. Electrochem, 1990]	42
Figure 4.5	Tube furnace (Model: Naber-Labotherm R70/9)	43
Figure 4.6	TP-270 solid source with Si wafer in quartz boat	44
Figure 4.7	The drive-in diffusion cycle for phosphorus [NOR Lab, School of Physics, USM]	46

Figure 4.8	Filmetrics F20	48
Figure 4.9	The vacuum coater unit	49
Figure 4.10	Spin-coating	51
Figure 4.11	The Mermert Oven 1130	52
Figure 4.12	The UV exposure system	53
Figure 4.13	Hard bake oven (Model Binder APT : Line Drying Oven)	54
Figure 4.14	The lift-off process flow	57
Figure 4.15	Annealing tube furnace	59
Figure 4.16	The solar simulator system	60
Figure 5.1	Thickness of Si wafers after thinning process in both techniques measurement	65
Figure 5.2	Graph of Si wafer thickness against wet etching time	65
Figure 5.3	AFM images at back surface Si wafers after thinning process	66
Figure 5.4	Back surface roughness RMS against etching time	67
Figure 5.5	Summary of sheet resistance, R_s and back surface roughness RMS of Si wafers against Si wafer thickness after thinning process	68
Figure 5.6	Thickness of SiO_2 against time of oxide grown	71
Figure 5.7	EDX spectra of Al BSF on back side Si substrate after alloying	72
Figure 5.8	FESEM images of alloying Al-BSF layer on the back side of Si substrate; a) at magnification 10k, b) at magnification 20k	74
Figure 5.9	Images of wafer from the effect in photoresist process where for a) spin speed of 2700 rpm; b) speed of 1000 rpm	77
Figure 5.10	Isolation scratches on the front surface for edge shunt isolation process	78
Figure 5.11	Result of open-circuit voltage before and after edge shunt isolation process	79

Figure 5.12	Result of short-circuit current before and after edge shunt isolation process	79
Figure 5.13	The <i>I-V</i> characteristics of illuminated (AM 1.5, 270 W/m ² , 25 °C) monocrystalline Si solar cell with various thicknesses of front surface passivation layer	82
Figure 5.14	Simulated results of spectral response of solar cell shows fall off in efficiency at high and low wavelengths for part of solar cell	84
Figure 5.15	Photogeneration contours in 2D solar cell. The center cathode electrode is opaque	87
Figure A.1	RCA clean solutions	97
Figure B.1	Solar cell mask	99

LIST OF ABBREVIATIONS

Abbreviation	Meaning
a-Si	Amorphous Silicon
Al	Aluminium
Al-BSF	Alloyed-Back Surface Field
Al-Si	Aluminium-Silicon
Al BSF	Aluminium doped back surface field
AM	Air mass
AM 1.5D	AM 1.5 Direct
AM 1.5G	AM 1.5 Global
ASTM	American Society for Testing and Materials
BOE	Buffered Oxide Etch
BSF	Back Surface Field
CdTe	Cadmium Telluride
CIS/CIGS	Copper Indium Gallium Diselenide
CVD	Chemical-Vapour Deposition
CZ	Czochralski
DI	Deionised water
FZ	Float Zone
GaAs	Gallium Arsenide
H ₂ O	Water
H ₂ O ₂	Hydrogen peroxide
H ₂ SO ₄	Sulfuric acid
HCl	Hydrogen chloride acid
HF	Hydrofluoric acid

I-V	Current-Voltage
IR	Infrared
ITO	Indium Tin Oxide
KOH	Potassium hydroxide
$\mu\text{c-Si}$	Microcrystalline Silicon
mc-Si	Multicrystalline Silicon
N_2	Nitrogen gas
NH_4OH	Ammonium hydroxide
NOR Lab	Nano-Optoelectronics Research Laboratories
P_2O_5	Phosphorus pentoxide
pc-Si	Polycrystalline Silicon
PECVD	Plasma-Enhanced Chemical Vapour Deposition
PERL	Passivated Emitter Rear Locally Diffused
PESC	Passivated Emitter Solar Cell
PV	Photovoltaic
PVD	Physical Vapor Deposition
RCA	Radio Corporation of America
sc-Si	Single-crystalline Silicon
Si	Silicon
SiO_2	Silicon dioxide
Si_3N_4	Silicon Nitride
TiO_2	Titanium Dioxide
UNSW	University of New South Wales
UV	Ultra violet light
Xe	Xenon
ZnO	Zinc Oxide

LIST OF SYMBOLS

Symbol	Meaning
α	Absorption coefficient
σ	Conductivity
σ_n	Electron capture cross section
σ_p	Hole capture cross section
λ	Wavelength
θ	Zenith angle
Ω/\square	Ohm per square
ρ	Space charge density
Φ	Electric potential
A	Area of the solar cell
As	Arsenic
B	Boron
B	Coefficient of radiative recombination
c	Speed of light
C_n	Auger coefficients for electrons
C_p	Auger coefficients for holes
D_n	Diffusion constants of electrons
D_p	Diffusion constants of holes
ϵ	Permittivity of material
ϵ_0	Permittivity of free space
eeh	Electron-electron-hole
ehh	Electron-hole-hole
E	Electric fields
E	Energy of photons

E	Incoming power from light illumination
E_C	Conduction band energy
E_g	Forbidden gap (band gap) energy
E_V	Valence band energy
F.F	Fill factor
G	Net generation rate
h	Planck's constant
I_L	Current density of illuminated light
I_{max}	Maximum current
I_n	Total current density for electron
I_p	Total current density for hole
I_{sc}	Short-circuit current
J_{sc}	Short-circuit current density
L	Diffusion length
μ_n	Mobility of electrons
μ_p	Mobility of holes
η	Efficiency
n	Concentration of free electrons
n_i	Intrinsic carrier concentration
n_{no}	Majority carriers of electrons at equilibrium
n_s	Concentration of electrons at surface
N_A^-	Density of ionized acceptors
N_D^+	Density of ionized donors
N_A	Ionized acceptor atom
N_C	Effective density of states in the conduction
N_D	Ionized donor atom
N_{dop}	Density of dopant atoms

N_V	Effective density of states in the valence band
N_t	Density of recombination centers
N_{ts}	Density of surface states per unit area
p	Concentration of free holes
p_{po}	Majority carriers of holes at equilibrium
p_s	Concentration of holes at surface
P	Phosphorus
P_{max}	Maximum power
R_s	Series resistance
R_{sh}	Shunt resistance
S	Surface recombination velocity
Sb	Antimony
S_{no}	Surface recombination velocity of electrons
S_{po}	Surface recombination velocity of holes
SRH	Shockley-Read-Hall
$\tau_{Auger,low}$	Low injection Auger lifetime
$\tau_{Auger,hi}$	High injection Auger lifetime
τ_{bulk}	Bulk lifetime
τ_n	Minority carrier lifetimes of electrons
τ_{no}	Minority-carrier lifetimes for electrons
τ_p	Minority carrier lifetimes of holes
τ_{po}	Minority-carrier lifetimes for holes
τ_{rad}	Radiative lifetime
$\tau_{rad,hi}$	High injection radiative lifetime
$\tau_{rad,low}$	Low injection radiative lifetime
τ_{SRH}	Shockley-Read-Hall lifetime
U	Net recombination rate

U_{Auger}	Auger recombination rate
U_{rad}	Radiative recombination rate
U_{SRH}	Shockley-Read-Hall recombination rate
v_{th}	Thermal velocity of charge carriers
V	Applied voltage
V_{D}	Diffusion voltage at equilibrium
V_{oc}	Open-circuit voltage
V_{max}	Maximum voltage
W	Width of the depletion region
Δn	Excess minority carrier concentration at p -side
Δn_{s}	Excess minority carrier concentration at the surface
Δp	Excess minority carrier concentration at n -side

KESAN PENGOKSIDAAN TERMA PADA KECEKAPAN SEL SURIA KRISTAL-TUNGGAL SILIKON

ABSTRAK

Tesis ini memberi fokus kepada fabrikasi monokristal sel suria silikon dan penekanan kepada pemaspifan permukaan di bahagian hadapan dan belakang sel diperhatikan. Objektif utama kajian ini adalah untuk membangunkan dan mengoptimumkan proses fabrikasi sel suria silikon. Perhatian khusus telah diberi untuk mencari ketebalan optima bagi proses pengoksidaan kering sebagai pemaspifan permukaan di hadapan dengan pertumbuhan terma untuk lapisan silikon oksida (SiO) telah disiasat untuk perbandingan. Teknik baru bagi mentafsir lapisan pemaspifan permukaan hadapan adalah dengan memperkenalkan kedua-dua proses pengoksidaan kering dan basah untuk membentuk lapisan oksida. Di samping itu, kesan tindak balas arus-cahaya daripada ketebalan oksida telah dikaji dengan menggunakan perisian SILVACO. Ciri-ciri belakang pemaspifan permukaan dengan mengoptimumkan filem Al-BSF telah dikaji secara meluas melalui pelbagai jenis rintangan. Rintangan berkurangan selepas pembentukan Al-BSF dari $\sim 6.05 \Omega \cdot \text{cm}$ kepada $\sim 1.81 \Omega \cdot \text{cm}$ untuk semua sel. Telah diperhatikan bahawa sel tanpa pemaspifan permukaan memberikan nilai output terendah dengan $V_{oc} = 383 \text{ mV}$, $I_{sc} = 5.25 \text{ mA}$ dan kecekapan hanya 0.29%. Sel terbaik dengan ketebalan oksida 905 \AA memberikan nilai kecekapan tertinggi iaitu 4.02% dan $V_{oc} = 468 \text{ mV}$, $I_{sc} = 24.70 \text{ mA}$. Nilai-nilai ini telah diuji dengan menggunakan sistem simulasi suria di bawah pencahayaan 270 W/m^2 dengan luas sel = 4.7 cm^2 di bawah AM1.5 pada 25° C .

THE EFFECT OF THERMAL OXIDATION ON MONOCRYSTALLINE SILICON SOLAR CELL EFFICIENCY

ABSTRACT

This thesis focuses on fabricating monocrystalline silicon solar cell and highlights the surface passivation on the front and back surface of the cell. The main objective of this work is to develop and optimize a process for the fabrication of silicon solar cell. Special attention has been paid to find the optimum thickness of dry oxidation process for front surface passivation with thermally grown silicon oxide (SiO₂) layers has been investigated for comparison. New technique for interpreting the front surface passivation layer is by introducing both dry and wet oxidation process to form the oxide layer. In addition, the effect of photocurrent response to oxide thickness is studied using SILVACO software. The rear surface passivation properties with optimised Al-BSF films have been extensively studied over a large range of resistivity. The resistivity decreases after the formation of Al-BSF from $\sim 6.05 \Omega \cdot \text{cm}$ to $\sim 1.81 \Omega \cdot \text{cm}$ for all the cells. It was observed that the cell with no surface passivation gives the lowest output value with $V_{oc} = 383 \text{ mV}$, $I_{sc} = 5.25 \text{ mA}$ and the efficiency only 0.29%. The best cell with oxide thickness of 905 \AA gives the highest efficiency value which is 4.02% and the $V_{oc} = 468 \text{ mV}$, $I_{sc} = 24.70 \text{ mA}$. The values were tested using solar simulator system under 270 W/m^2 illumination with cell area = 4.7 cm^2 under AM1.5 at $25 \text{ }^\circ\text{C}$.

CHAPTER 1

INTRODUCTION

1.1 Renewable Energy Sources

Renewable energy sources are energy sources that are continually producing energy. The sources are from sun, water, wind, geothermal and biomass. On the other hand, fossil fuels such as coal, oil and natural gas are categorizing in non-renewable energy sources. The function of both renewable and non-renewable energy sources are used to generate electricity and power for vehicles or machines.

The renewable energies are non-polluting and environmentally friendly. Even though renewable energy sources are categorized in a free source (because it is from natural sources) but still there are some positive and negative impacts to the environment. The list of advantages and disadvantages for every renewable energy source are as in Table 1.1.

Table 1.1 Renewable energy sources

Energy Source	Types of Process	Advantages	Disadvantages
Solar thermal	Direct heating and cooling from solar radiation absorption	Non-polluting, unlimited energy source	Big storage required
Solar photovoltaic	Sunlight is directly convert into electricity via semiconductor materials	Non-polluting, unlimited energy source, relatively maintenance free	Operating lifetime, high cost of cells
Hydroelectric	Building a dam to let the water flow through it to generate electricity	Non-polluting, inexpensive	Limited to special locations, cause damage to existing habitats
Tidal	Motion of water by gravitational pull of moon used to generate electricity	Non-polluting, inexpensive	Do not produce a lot of electricity, limited number of exploitable sites
Wind	Force of the wind used to generate electricity	Non-polluting	Winds blow are intermittent, limited to special locations, big storage required, noisy
Wave	1) Directs waves into man-made channels; water passes through a turbine and generates electricity 2) Wave are moves up and down to push air	Non-polluting, not affect wildlife, wave turbines operate in quiet conditions	Wave heights vary considerably so that it could not produce constant supply of energy
Geothermal	Decaying of radioactive materials within the earth to produce the heat	Inexpensive	Limited to special locations, corrosion problems

Typically, electricity uses fossil fuels. However, fossil fuels are a non-renewable energy source, meaning with the use of these fuels the Earth's supply depletes. Solar energy is the source of nearly all energy on the earth. Humans, animals and plants rely on the sun for warmth and food. However, people also harness the sun's energy in many other different ways. For example, biomass converts the sun's energy into a fuel, which can then be used for heat, transport or electricity. Wind energy used for hundred of years to provide mechanical energy or for transportation, uses air currents that are created by solar heated air and the rotation of the earth. Hydroelectric is also derived from the sun, depends on the evaporation of water by the sun and its subsequent return to the Earth as a rain to provide water in dams. Photovoltaic is a simple and elegant method of harnessing the sun's energy. So that, from Table 1.1, solar photovoltaic devices (solar cell) are unique in that they directly convert the incident solar radiation into electricity, with no noise, pollution or moving parts, making them robust, reliable and long lasting. These makes photovoltaic energy are preferred as a useful energy source for the future.

1.2 The Role of Solar Photovoltaic Energy

Photovoltaic (PV) energy is also known as solar energy elected as useful contributor to our future needs. However, this type of energy source still need to be improved in some certain area in order to achieved high performance. The current solar cell fabrication must excel in cost reduction, high efficiency and operating lifetime to make photovoltaic energy be useful worldwide.

The first generation of solar cell consists of single-crystalline (sc-Si) and polycrystalline (pc-Si) wafer-based silicon (Si). These first generation solar cells dominate the market with their best promising in high efficiency compare with other generations. For

sc-Si solar cell, the cell shows the highest in the efficiency which is around 20-24%, follow by the pc-Si solar cell at 14-18% at air mass 1.5. However, the cost of production due to basic materials (i.e. Si wafer) is relatively high (<1.4 USD/W). The methods such as Czochralski (CZ) and Float Zone (FZ) are use to produce high purity sc-Si and pc-Si wafers respectively, make the costs of production high [Mahajan, S. & Harsha, K. S. S., 1999]. The sc-Si solar cell shares the highest percentage in market for years of 2009 and 2010 compares to the others technology, showing that this cell is more promising in the marketing.

Second generation thin-film solar cell technology consists of amorphous silicon (a-Si), copper indium gallium diselenide (CIS/CIGS) and cadmium telluride (CdTe) is promising in low cost due to materials and productions. This generation is still modest in industrial market compare to the first generation, although it has low cost in productions (~0.9 USD/W). This is because they are struggling to compete with sc-Si solar cell module prices and facing problems in material durability, availability and toxicity (in the case of Cadmium) [IRENA, 2012]. Furthermore, the confirmed solar cell efficiency at air mass 1.5 are still low which is around 6-12%. However, this second generations technology showing reduction in PV module size to as small as 0.6 m².

The third generation technologies are not yet to be commercialized at any scale and said still in research and development (R&D) phase, but it has high potential in low cost, weight and free-form shaping. The manufacturing of third generation are same with the second since they are based on thin films technology but lie on advanced concepts of solar cell (advanced thin films). The third generation of solar cell technology are consists of III-V compound multijunction, concentrated PV (CPV) and organic or polymer (OPV). They are still in research stage; the researcher from UNSW conducted research on all Si tandem cell based on band gap engineering of Si in amorphous matrix (oxides, nitrides and carbides)

[Conibeer, G., et. al., 2008], conversion via up and down of photon, and hot carriers effects in solar cell [Konig, D., et. al., 2010].

Table 1.2 Overview and comparison of major PV technology

		1 st Generation PV		2 nd Generation PV			3 rd Generation PV	
Technology	Units	Single crystalline silicon (sc-Si)	Poly-crystalline silicon (pc-Si)	Amorphous silicon (a-Si)	Copper Indium Gallium Diselenide (CIS/CIGS)	Cadmium Telluride solar cells (CdTe)	III-V compound Multi-junction, Concentrated PV (CPV)	Organic or Polymer (OPV)
Confirmed solar cell efficiency at AM1.5	%	20-24	14-18	6-8	10-12	8-10	36-41	8.3
Commercial PV Module efficiency at AM1.5	%	15-19	13-15	5-8	7-11	8-11	25-30	1
Current PV module cost	USD/W	<1.4	<1.4	~0.8	~0.9	~0.9	-	-
Market share in 2009	%	83	3	1	13	-	-	-
Market share in 2010	%	87	2	2	9	-	-	-
Maximum PV module output power	W	320	320	300	120	120	120	-
PV module size	m ²	2.0	1.4-2.5	1.4	0.6-1.0	0.72	-	-
Area needed per kW	m ²	7	8	15	10	11	-	-
State of commercial-ization		Mature with large-scale production	Mature with large-scale production	Early deployment phase, medium-scale production	Early deployment phase, medium-scale production	Early deployment phase, small-scale production	Just commercialize small-scale production	R&D phase

1.3 Scope of Study

The thin silicon oxide grown layer will be studied in term of passivation layer on the front surface of Si solar cell. The different thickness of oxide layer will be studied in order to see the effect to the output voltage and the conversion efficiency. The best method for back surface field (BSF) was also investigated.

The relation between the spin speeds from photolithography process to the pattern created from lift-off process is investigated. The difference in spin speed and time of speed affects the lift-off process.

In the present study, solar cell will be fabricated using monocrystalline <100> Si wafer. This is follow by creating the emitter layer on the front and the thin passivated oxide layer. The other process such as metallization, annealing, back surface field, alloying and shunt isolation will be investigated. For doping process, the solid source will be used all along this study due to its uniform doping and clean resulting surface compared to the spin-on-doping.

1.4 Research Objectives

The objectives of this study are as follows:

- 1) To study the effect of combination wet and dry oxidation process to the formation of front surface passivation layer.
- 2) To study the effect of thin oxide passivated layers to Si solar cells performance.
- 3) To investigate the performance of Si solar cells such as I_{sc} , V_{oc} , F.F and efficiency.

1.5 Thesis Organization

Chapter 1 explains the different types of renewable energy source and the role of the solar cell for the future compare with other sources. The scope and research objectives also outlined in this chapter.

Chapter 2 outlined the genealogy of silicon solar cell, the surface passivation of silicon solar cell, thin passivating oxide film and rear passivating back surface field.

Chapter 3 explains the basic principles of Si and solar cell. In this chapter also explains the relevant theories related in solar cell performances.

Chapter 4 presents the methods and equipments used in this study. The methods such as RCA clean, diffusion, thermal oxide passivation layer on the front surface, back surface field passivated layer on the rear surface, alloying, photolithography, metallization, lift-off, shunt isolation, annealing, *I-V* measurements and SILVACO simulation are discussed briefly. All of this fabrication processes are carried out in Nano-Optoelectronics Research Laboratories (NOR Lab) in the School of Physics, Universiti Sains Malaysia.

Chapter 5 discussed about experimental observations, calculations and the results of this study. The final result and the effect of efficiency also will be discussed in this chapter.

Chapter 6 concludes the findings of this study, followed by some recommendation for future works on fabrication of Si solar cell.

CHAPTER 2

LITERATURE REVIEW

2.0 Introduction

This chapter aims to investigate the tendency of the existing works related to silicon solar cell generally and the study of surface passivation particularly, that have been explored by previous researchers. The works are highlighted and summarized to seek the means of the conceptual framework. The study of the silicon solar cell has been examined by various researchers. Focus of this chapter has generally been divided into four main themes in this work highlights. It begins with a discussion about related works of silicon solar cell. Further discussion focused on the surface passivation as subjects where the thin passivating oxide film and rear passivating back surface field are briefing in details. Accordingly, the results from previous works are highlights. A framework has been made to study the principles for the purpose of investigation.

2.1 Genealogy of Silicon Solar Cell

In 1954, the first modern Si cell was developed by Chaplin, Fuller and Pearson at Bell Telephone Laboratories. They claimed that current is generated when diffused *p-n* junction devices were exposed to light [Chaplin, et. al., 1954]. Lithium was used for diffusion source to form a junction and recorded the efficiency of about 4.5% [Pearson, G. L., 1985]. After this encouraging recovery, the lithium diffusion was replaced by boron and the efficiency rose to 6% [Bell lab., 1954]. Later, the efficiency value went up to 10% due to the

improvement made to the 1cm x 2cm cell structure by introduced the shingling contact [Bell lab., 1955].

The sizes of cell were decreased to 0.5cm x 2cm and that lowered the series resistance compare to previous cell size type. The average conversion efficiency reached 8.5% in 1957. In 1961, the cell development for space applications was encouraging the researchers to improve the metal contact grids on the top surface by introducing the front contact strip over the active surface and recorded an increase in efficiency to 11% [Maldelkorn, J., et. al., 1962]. This reduced the series resistance. In 1963, the next milestones is in junction formation where boron-doped forming p - n junction was change to more radiant-resistant phosphorus-doped; n - p junction. However, these cell result in decreasing cell efficiency to 10%.

In the first 1970s, several innovations on the cell design were introduced by many researchers. The development in violet cell marked an advance for 2cm x 2cm of 10 ohm.cm n - p cells. Reduction in junction depth from 4000 Å to 1500 Å eliminated the dead layer [Mandelkorn, J., et. al., 1973]. Another important invention; back surface field (BSF) was announced by Mandelkorn and Lamneck in 1972 by deposited p^+ impurity (such as aluminium) into the rear side of Si wafer. The BSF improved current and voltage output by getter the impurities in the cell bulk [Iles, P. A., 1970]. This was explained in terms of highly doped p -type layer formed at the rear surface by the effect of alloyed aluminium [Mandelkorn, J., et. al., 1973]. The heavily doped aluminium region suppresses the minority carrier concentrations on the rear surface of the cell and thus restricting the recombination. The gettering effect of rear aluminium treatments has also been established [Pasquinelli, M. et. al, 1991]. The BSF reduces in the effective minority carrier recombination velocity at the back side [Narayan, S. et. al., 1989].

Further improvements were announced in 1974 at COMSAT Laboratories where the black cells were introduced [Fred, T., 1998]. The selective etching schemes at the front surface are introduced to form the light-trapping pyramids to eliminate the reflection losses [Ritter & Arndt, 1976]. A combination of violet and black cell technologies with BSF led to increase the efficiency to 15%.

The next improvement was due to passivated the top surface of the cell with thermally grown oxide; resulted increasing in output voltage. The passivated emitter solar cell (PESC) reduced the area of contact on the top surface and minimizes the activity at the interface with the top metal contact. At 1985, an efficiency of 20% was recorded [Green, M. A., et. al., 1985].

Based on the encouraged result of the passivation from previous studies, the next major advance in cell design resulted from extending the oxide passivation to both front and rear surfaces of the cell were recorded. The first successful design in point contact was published [Sinton, et. al., 1985]. The design were improved by localized the contacts to small points on the non-illuminates surface and then reduced the effect of contact recombination at the top surface. Processing the cell presents challenges in the terms of defects from the oxide created because it can cause the shunting between the rear contacts and the substrate [Sinton, R. A., et. al., 1990]. These highly innovative cells record the efficiency of 22% under normal terrestrial testing and increased to 27% under highly concentrated sunlight [Sinton, R. A., et. al., 1986]. The passivated emitter rear locally diffused (PERL) solar cells; the combinations of the two previous designs were recorded to be the highest efficiency above 23% [Green, M. A., 1991].

2.2 Surface Passivation

In the 1980's, advances in the passivation of both cell surfaces led to the first crystalline Si solar cell with conversion efficiencies above 20%. With today's industry trend towards thinner wafers and higher cell efficiency, the passivation of the front and rear surfaces is now also becoming vitally important for commercial Si solar cell.

Thus, it make the researcher becomes interest in the Si solar cell passivation surfaces field. Improving the cell efficiency and introducing new method in surface passivation is the aim. Modern structure of Si solar cell via passivated the front and rear surface are introduced. In high-efficiency Si solar cell, decreasing the surface recombination losses is highly suppressed by introducing the methods of growing thin silicon dioxide (SiO_2) film at the front surface and deposited highly-doped aluminium layer of back surface field (Al BSF) at the rear surface.

2.3 Thin Passivating Oxide Film

The most fundamental issue by using Si as a substrate is its low ability in absorbing light since it has low absorption coefficient (α) near infrared (IR). Moreover, Si is indirect band gap semiconductor [Brendel, R., 2005]. To overcome its ability in poor absorption, the method of passivated the front surface is introduced in order to achieve high value in conversion efficiency.

The incident light can be utilized more effectively in solar cell device by incorporating the passivating layer on top of the device; typically by SiO_2 , silicon nitride (Si_3N_4), zinc oxide (ZnO), indium tin oxide (ITO) or titanium dioxide (TiO_2) [Müller, J., et.

al., 2004, Yang, W., et. al., 2010]. The purpose of this thin passivating layer is to reduce the surface recombination velocity [Fossum, J. G. & Burgess, E. L., 1978].

Growing SiO₂ at high temperature (≥ 900 °C) in oxidation process is very effectively method in order to gain high efficiency in Si solar cell laboratory [Zhao, J., et. al., 1999]. In many industrial, high-temperature oxidation is not a choice in fabrication because of the high sensitivity of the Si bulk lifetime to high-temperature processes. It leads to degradation of the bulk lifetime [Stocks, M. J., et. al., 1997] which leads to increase the surface recombination velocity. Silicon nitride (SiN_x) grown by plasma-enhanced chemical vapour deposition (PECVD) at ~400 °C was chosen as alternative which has resulted in low surface recombination velocity. However, the short-circuit current density value reduced compared to SiO₂ passivated [Dauwe, S., et. al., 2003].

The first Si solar cell with oxide passivation layer on the top surface of the cell was fabricated in 1960's [Riordan, M. & Hoddeson, L., 1997]. This device gives a surprisingly large photovoltage and cell of close to 15% energy conversion efficiency had been demonstrated. The next phase of activity resulted in improvement in photolithography, texturing on the front cell surfaces and passivated the rear surface of the cell. In the middle of 1970's, cell efficiency of close to 17% with oxide passivation layer on the front surface had been demonstrated. In the 1980's, surface passivation using thin layer of oxide improved the efficiency above 20% [Blakers, A.W. & Green, M. A., 1999].

In this study, in order to gain high efficiency of Si solar cell, the method of growing thin passivating oxide film at high temperature is investigated. However, the method of growing thin film is different from the previous works where wet drive-in method is introduced in this works. These differences are then being compared by its efficiency output values.

2.4 Rear Passivating Back Surface Field

In most industrial Si solar cell fabrication, the back surface is improved by introduced the back surface field (BSF). To obtain effective BSF, doping concentration at the rear surface should be high ($> 10^{17} \text{ cm}^{-3}$) and the thickness of the BSF should be around 1 μm . Doped aluminium (Al) layer at the rear surface improved the BSF compared with boron doped. Al-doped as BSF increased the efficiency of Si solar cell by about 10% [Koval, T., et. al., 1996]. The BSF acts by decreasing the surface recombination velocity and hence increases the minority carrier diffusion length in the base Si solar cell. In industry, Al paste is used to deposit the BSF and excellent result in electrical characteristics is achieved by thinning the wafer [Khadilkar, C., et. al., 2005]. While in laboratory, normally Al was evaporated at the rear surface to form the Al layer.

Thick Al layer of BSF will causes severe warping to Si wafer with thickness less than 250 μm . This warping gives difficulties in subsequent production processes and increases the breakage of the cells [Preu, R., et. al., 2002]. So that the thickness of Al layers between 0.1 and 0.2 μm were investigated at heated temperature of 800-1000 $^{\circ}\text{C}$. They give the results of increasing in short-circuit current [Harttley, N. O., et. al., 2002].

The formation of Al-Si alloyed layer at Al-BSF is well known give the advantage in high conversion efficiency. Due to the presence of Al alloying gave the effect of reflector for minority carrier at the back surface and recorded the efficiency of 19.1% [Doshi, P., et. al., 1997] by applying of 10 μm evaporated Al-BSF on the multicrystalline Si solar cells and efficiency of 17.5% has been obtained with 2 μm evaporated Al-BSF on monocrystalline Si solar cells [Peters, S., et. al., 2002].

In view of the above, I have carried out rear surface recombination passivation by alloying aluminium after depositing a 1 μm evaporated aluminium layer. Thick Al layer and

high alloying temperatures (over 800 °C) is necessary in order to obtain low values of surface recombination velocity that contributes to high value in output.

2.5 Summary

Surface passivation of solar cell has been studied by several researchers in many years. Even though there are many studies about oxide layer as surface passivation, but so far there are still less in research about the effects of variable oxide surface passivation thickness to solar cell efficiency. This study focuses entirely on the effects of variable oxide surface passivation thickness to solar cell efficiency.

CHAPTER 3

THEORY

3.0 Introduction

This chapter discusses about the theories that have been used in order to achieve the objectives of this study. In general, the theory of Si, solar cell characteristics and surface passivation are discussed in details to support the idea in fabricating solar cell. The *p-n* junction behaviour, *I-V* characteristics and relevant equations have also been discussed in this chapter. The theory contained in this chapter is used to collect and analyze the data.

3.1 Theory of Silicon

Silicon, Si is located in group IV element in periodic table which adopts the tetrahedral or diamond crystal structure at room temperature and pressure (Figure 3.1). Every valence electron of Si is involved in bonding. The band gap of Si is indirect band gap where the value of band gap energy is 1.12 eV at room temperature. This band gap value is fairly close to the optimum for solar energy conversion which is ~1.4 eV [Nelson, J., 2003]. Si refractive index is 3.5 and the reflectivity over the visible wavelength is about 30%. A single or multilayer anti-reflection coating introduced in order to reduce the reflectivity effect to less than 5%. So far, Si still appears to be the best material in fabrication solar cells due to its abundance (about 25% of silica in the earth's crust), band gap close to optimum, non-toxicity, proven product durability and good electronic properties [Green, M. A., 1995].

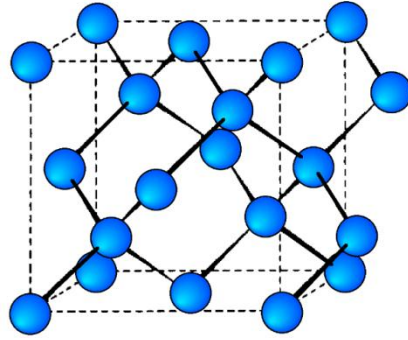


Figure 3.1 Tetrahedral crystal structure of crystalline silicon

Figure 3.2 shows the schematic diagram for electrons transition in semiconductor. E_v is maximum energy of the valence band and E_c is the minimum energy of conduction band. In order to conduct the electricity, electrons must be free with minimum energy (band gap energy) to make transition (excite) from E_v to E_c .

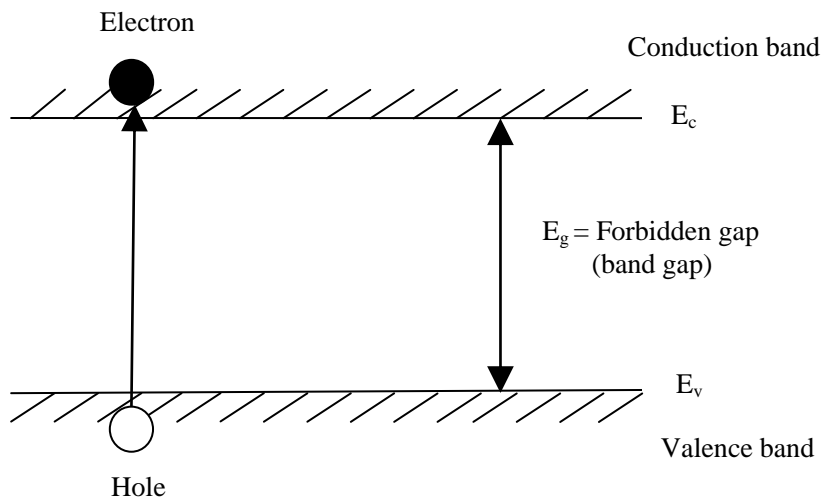


Figure 3.2 The schematic diagram of energy bands for electrons in a semiconductor

There are various types of crystalline Si which is differentiated by its grain size and the ordered of the crystal structure. For monocrystalline Si (sc-Si), the grain size is > 10 cm and the common growth technique is by Czochralski (CZ) or float zone (FZ). While for

multicrystalline Si (mc-Si) have a grain size of 1 mm – 10 cm with the growth techniques by cast, sheet or ribbon. The grain size for polycrystalline Si (pc-Si) is 1 μm – 1 mm and the growth technique is by chemical-vapour deposition (CVD). For microcrystalline Si ($\mu\text{c-Si}$), the grain size is $< 1 \mu\text{m}$ with plasma deposition is their growth technique. On the other hand, amorphous Si (a-Si) is characterized by short range order of atomic periodicity in the Si lattice. From top of the above terminologies, monocrystalline Si are used as substrate material for this experiment that will discuss later in the next chapter.

3.2 Theory of Solar Cell

3.2.1 The p - n Junction

In order to understand how a solar cell works, understanding of p - n junction structure is needed. A p - n junction is established when joining the p -type and n -type of the semiconductor materials into contact with each other. The electrons or holes in p - n junction move because of the concentrations gradient different. Since the n -type region has high in electron concentrations compare to p -type region, electrons diffuse from the n -type side to the p -type side. Similarly, the p -type region has high in hole concentrations compare to n -type region. The holes flow by diffusion from p -type side to the n -type side. However, such diffusion cause positive charge appears on the n side and negative charge on the p side. As a result, an electric field is formed and the region where the electric field formed are called depletion region. Figure 3.3 shows the structure of p - n junction.

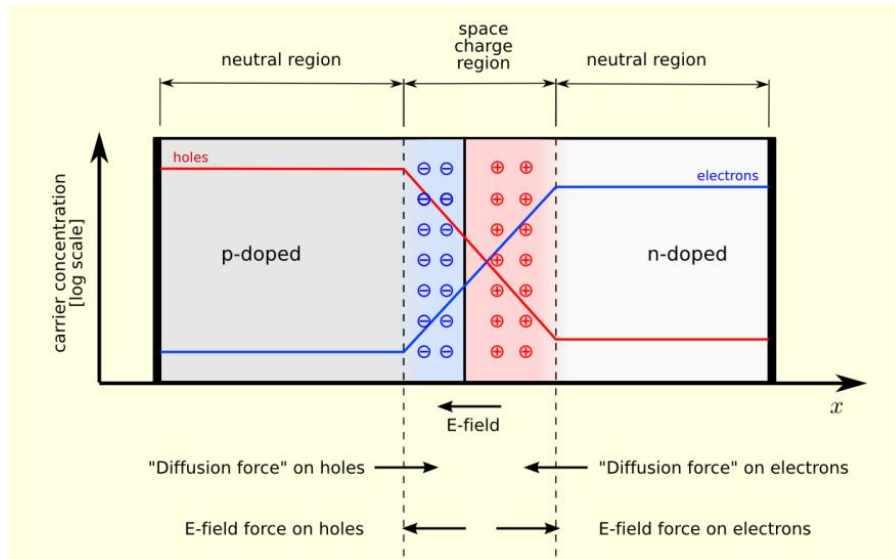


Figure 3.3 The p - n junction structure

3.2.2 The p - n Junction at Equilibrium

As discussed before, p - n junction consists of p -type and n -type material in contact with each other. In thermal equilibrium conditions, there are no external input connected into the junction; either by voltage, extra heat, or light. When n -type and p -type material comes into contact, electrons (majority carriers) diffuse from n -type into p -type side and leave behind the uncompensated donors, N_D in the n -type region. Similarly, holes (majority carriers), where the uncompensated acceptors, N_A are leave in the p -type region when holes diffuse from p -type into n -type region. The flowing of electrons and holes across the junction results the current diffusion. From the formation of N_D and N_A , they set up an electric field and create the drift current in the opposite direction to the diffusion current. Under equilibrium conditions, the net current is zero. So that, carriers in the diffusion current keeps moving until the sum of the diffusion current and the drift current for both electrons and holes are zero.

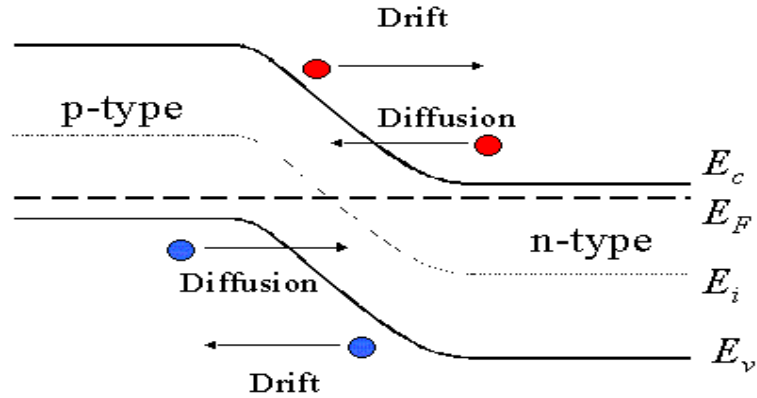


Figure 3.4 Energy band diagram of a p - n junction in thermal equilibrium

The space charge region is said to be in thermal equilibrium when the currents condition is balanced. The electric field acts as a barrier to prevent the electrons to keep moving across the junction from n to p regions. The majority carriers are dominant carrier type where for electrons in n region, $n_{no} \gg p_{no}$ and for holes in p region $p_{po} \gg n_{po}$. The concentrations of n_{no} and p_{po} at room temperature are given by the density of ionized dopants which is

$$n_{no} \approx N_D, \quad p_{po} \approx N_A \quad (3.1)$$

The law of mass action is states that $n_i p_i = n_i^2 = np$ at any point in the semiconductor. From Boltzmann equation, the free carrier concentration of electrons and holes at thermal equilibrium are

$$n = N_C \exp\left(-\frac{E_C - E_F}{kT}\right) \quad (3.2)$$

$$p = N_V \exp\left(-\frac{E_F - E_V}{kT}\right) \quad (3.3)$$

Where:

N_C = Effective density of states in the conduction

N_V = Effective density of states in the valence band

So that, the intrinsic carrier concentration, n_i can be described as

$$n_i^2 = n p = N_c N_v \exp\left(-\frac{E_g}{kT}\right) \quad (3.4)$$

where E_g is the energy band gap between the conduction and valence band ($E_c - E_v$).

Therefore, the built in voltage, V_D at equilibrium is

$$V_D = \frac{kT}{q} \ln\left(\frac{N_D N_A}{n_i^2}\right) \quad (3.5)$$

3.2.3 The p - n Junction at Non-Equilibrium

The p - n junction is said to be in non-equilibrium state if voltage, V is applied to the junction or light is incident to the junction ($np > n_i^2$). As a result, the minority carrier concentration and the net carrier density are changed. The recombination rate of minority carriers proportional to the excess minority carrier concentration which is Δn from p -side and Δp at n -side.

In this case, the current density at the quasi-neutral region of p - n junction becomes

$$J_n = qD_n \frac{dn}{dx} \quad (3.6)$$

$$J_p = -qD_p \frac{dp}{dx} \quad (3.7)$$

and the total current density is

$$J(x) = J_o \left(e^{\frac{qV}{kT}} - 1 \right) \quad (3.8)$$

Where J_o is the saturation current density and J_o is given by

$$J_o = \frac{qD_n n_i^2}{L_n N_A} + \frac{qD_p n_i^2}{L_p N_D} \quad (3.9)$$

and L is the diffusion length;

$$L = \sqrt{D\tau} \quad (3.10)$$

3.2.4 The p - n Junction under Illumination

When the p - n junction is illuminated, electron-hole pairs are generated in semiconductor. Total current density is a sum of current density in dark conditions and illuminated, J_L . Therefore,

$$J = J_o(e^{qV/kT} - 1) - J_L \quad (3.11)$$

Solar cell becomes an open circuit when no external contact was attached between p and n -type region. Thus, the current density in the dark condition changes to under light condition. Consequently, the current density increases when the V_D decreases with increasing the amount of open-circuit voltage, V_{oc} as in Equation (3.12);

$$J_L = J_o \exp\left(\frac{-q(V_D - V_{oc})}{kT}\right) \quad (3.12)$$

This equation is the generation current under illumination condition where the photo-generated electron current is collected in the n -type region. This current flows to the back region by the external load.

3.3 Photovoltaic Effect

The photovoltaic effect is the basic physical process through which a photovoltaic, PV cell (i.e. solar cell) converts sunlight into electricity. From quantum theory, sunlight is composed of photons—packets of solar energy. These photons contain different amounts of energy that correspond to the different wavelengths of the solar spectrum [Nelson, J., 2003]. When photons strike a PV cell, they may be reflected or absorbed, or may pass through it. Some of the absorbed photons generate the electricity. The energy of a photon is transferred to an electron in solar cell (semiconductor device). When the electrons gain its new energy, it become mobile and able to escape from its normal position associated with a single atom in the semiconductor to become part of the current in an electrical circuit. Special electrical property of the PV cell is a built-in electric field provides the voltage needed to drive the current through an external load. Since the voltage is produced from the action of photons, the term Photovoltaic is used to describe the process in a PV solar cell.

Figure 3.5 illustrates the basic operation of solar cell. In order to generate power from the cell, voltage has to be generated as well as current. Light photons are absorbed by the semiconductor and in the process generate electric-charge carriers called electrons and holes. After the generation of electrons and holes, they diffuse to $p-n$ junction where the electrons are swept away to n -type material whereas holes are swept away to p -type material causing charge separation and make existent of strong internal electric field.

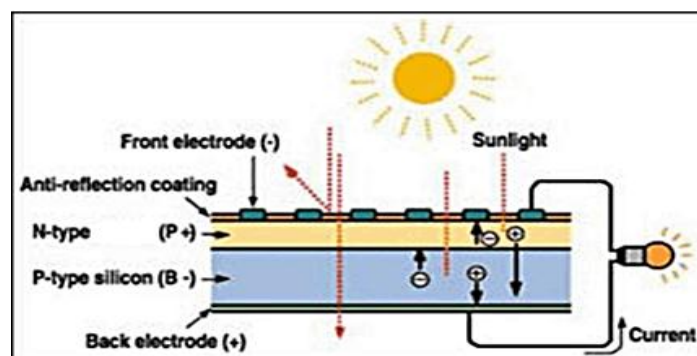


Figure 3.5 Schematic diagram of photovoltaic effect in solar cell

3.4 Air Mass and Solar Spectrum

3.4.1 Air Mass

The solar spectrum and irradiance is authorized by the air mass. Air mass, AM is related to the optical path length through earth's atmosphere where the direct sunlight has to pass through before it reaching the earth's surface. It is determined by the angle, θ that the sun makes with a vertical line perpendicular to the horizontal plane (Figure 3.6). It is given by

$$\text{Air mass (AM)} = \frac{1}{\cos \theta} \quad (3.13)$$

Where:

θ = Angle with respect to the surface normal (zenith angle)

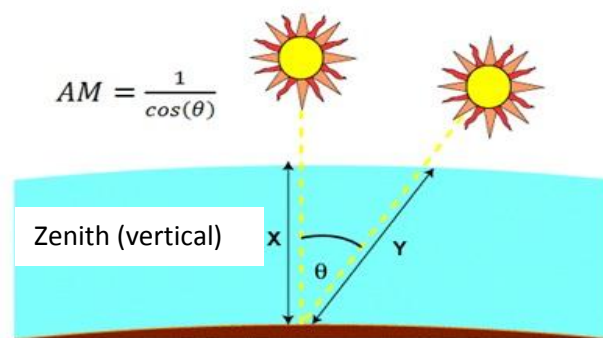


Figure 3.6 The air mass

AM 0 correspond to the solar spectrum in the outer space because there is no light pass through the atmosphere at this stage and is applicable for satellites. When the sun is directly overhead, the AM is 1. While when the angle of the sun from zenith increases, the AM increases. So that at $\theta = 48.2^\circ$, the AM is 1.5. Under standard test condition, STD for

solar cell, AM 1.5 is used as reference [Nelson, J., 2003]. AM 1.5 are divided into two which is AM 1.5 Global (AM 1.5G) and AM 1.5 Direct (AM 1.5D). The AM 1.5G spectrum is designed for flat plate modules and has an integrated power of 1000 W/m^2 (100 mW/cm^2). The AM 1.5D (+circumsolar) spectrum is defined for solar concentrator work.

3.4.2 Solar Spectrum

Figure 3.7 shows the spectral irradiance of the sun (from ASTM G173-03 reference spectra) with wavelength from ultraviolet, UV to infrared range is present. The spectrum of the sun's solar radiation is close to that of a black body with a temperature of about 5800 K. It can be seen from the figure, the spectrum peak which is around 600 nm.

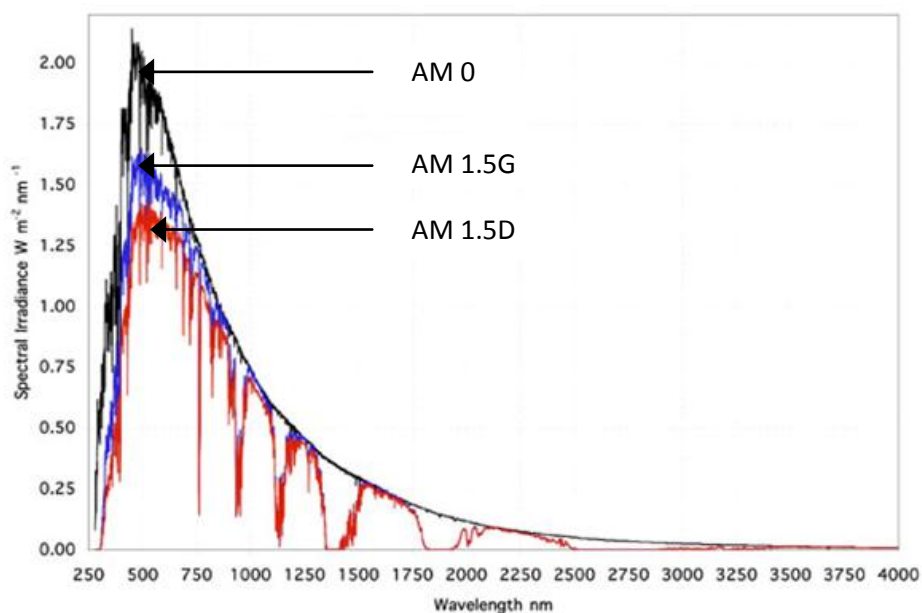


Figure 3.7 Spectral irradiance of the sun under AM 0, AM 1.5G and AM 1.5D